3D Printable Linear Soft Vacuum Actuators: Their Modeling, Performance Quantification and Application in Soft Robotic Systems

Charbel Tawk, Geoffrey M. Spinks, Marc in het Panhuis, and Gursel Alici

***Abstract*—Conventional robotic systems have proved their versatility in the industry where complex tasks requiring high force, high speed and high precision are desired. However, these rigid-bodied systems cannot collaborate safely with humans. Soft robots which are primarily made of highly compliant materials bring robots and humans together by operating safely in unstructured environments. Soft robots demand dexterous soft actuators that preserve or enhance their softness and safety features. This article reports on modeling, performance quantification, and soft robotic applications of directly three-dimensional (3-D) printed linear soft vacuum actuators (LSOVA), that are manufactured in a single step, using a low-cost and affordable open-source fused deposition modeling 3-D printer. Numerical and experimental results presented show that LSOVA have multiple advantages including high bandwidth (∼6.49 Hz), high output force (∼27 N) and long lifetime (∼21 500 cycles). LSOVA blocked force and linear stroke can be predicted accurately using finite element and analytical models. Furthermore, LSOVA are scalable. The soft actuators can be either assembled in parallel as a bundle, where a linear relationship exists between the number of actuators and the output force or can be scaled up in terms of internal volume where a linear relationship exists between the output force and the internal volume of a single actuator. Finally, LSOVAs were tailored for various robotic applications including soft crawling robots for navigation in tubular systems, soft parallel manipulators for pick and place tasks, soft artificial muscles, soft prosthetic fingers for prosthetic hands, and soft adaptive grippers for gripping applications.**

***Index Terms*—Artificial muscle, gripper, manipulator, prosthetics, soft actuator, soft robotics.**

Manuscript received April 14, 2018; revised January 8, 2019 and March 25, 2019; accepted July 28, 2019. Date of publication August 5, 2019; date of current version October 15, 2019. Recommended by Technical Editor J. C. Koo. This work was supported in part by the ARC Centre of Excellence for Electromaterials Science under Grant CE140100012 and in part by the University of Wollongong, Australia. *(Corresponding author: Gursel Alici.)*

C. Tawk and G. Alici are with the School of Mechanical, Materials, Mechatronic, and Biomedical Engineering, and ARC Centre of Excellence for Electromaterials Science, University of Wollongong, Wollongong, NSW 2522, Australia (e-mail: ct887@uowmail.edu.au; gursel@uow.edu.au).

G. M. Spinks is with the Intelligent Polymer Research Institute, ARC Centre of Excellence for Electromaterials Science, University of Wollongong, Wollongong, NSW 2522, Australia (e-mail: gspinks@uow.edu.au).

M. in het Panhuis is with the Soft Materials Group, School of Chemistry and Intelligent Polymer Research Institute, and ARC Centre of Excellence for Electromaterials Science, University of Wollongong, Wollongong, NSW 2522, Australia (e-mail: panhuis@uow.edu.au).

This article has supplementary downloadable material available at http://ieeexplore.ieee.org, provided by the authors.

Color versions of one or more of the figures in this article are available online at http://ieeexplore.ieee.org.

Digital Object Identifier 10.1109/TMECH.2019.2933027

I. Introduction

ROBOTS are becoming smarter and more capable of performing complex tasks due to recent technological advancements. These smart systems are widely used in the industries that rely on repetitive and laborious tasks involving high precision, high accuracy, large forces, and high speeds [1]. One main drawback of these conventional robots is their inability to operate alongside humans. These robotic systems are made of rigid materials and components that make them unsafe to operate in unstructured environments [2]. To extend the robot applications beyond classical automation tasks to tasks requiring interaction between the robots and their operation environments, it is essential to have a safe and conforming interaction between robots and humans. Soft robots which are made of highly compliant and deformable materials are a tangible solution to bringing robots and humans closer as task partners since soft robots are purposefully designed to operate in unstructured environments. Soft robots are inspired by soft biological structures, such as octopus arms, squid tentacles, elephant trunk, and worms [3]. Ideally, a soft robot should be made primarily of soft materials where the mechanical structure, actuators, sensors, power source, and electronics are compliant and deformable, and if possible, they should be incorporated seamlessly in the same continuum body. However, it is very challenging to develop such soft robots that incorporate all these features and still provide useful performances.

Establishing the soft actuation concept and its realization is the first and most important step in building a soft robot. Soft robotic systems demand dexterous soft actuators that can facilitate the soft and adaptive interaction between the robots and their environments. Therefore, significant research efforts have recently been dedicated to developing soft actuators and artificial muscles that can be used to articulate soft robots. To this aim, smart materials and structures such as shape memory alloys [4]–[8], dielectric elastomers [9], [10], ionic polymer-metal composites [11], coiled polymer fibers [12], [13], hydrogels [14], [15], humidity-responsive materials [16], and magnetic responsive structures [17] have been used to establish

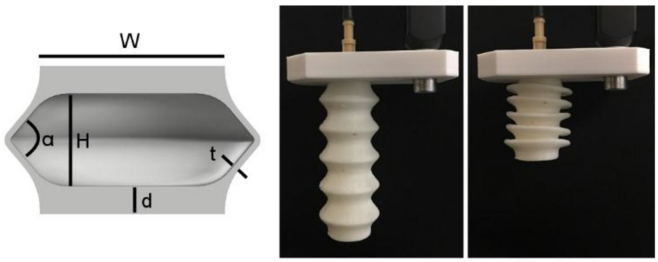

(a) (b) (c)

Fig. 1. LSOVAs. (a) Dimensions and the cross-sectional view of a 1C–LSOVA. W: 20 mm, H: 10 mm, d: 3 mm, t: 0.90 mm, α: 110°—these dimensions are the same for each cell of the actuator. (b) Initial position of a 5C–LSOVA when no vacuum is applied. (c) Final position of 5C–LSOVA when 95.7% vacuum is applied (see Table I).

actuation concepts for soft robots. Chemical reactions, such as combustion [18], electrolysis [19], and catalytic reactions [20] have been integrated within soft robots and soft structures as energy sources to drive them. Phase-change materials such as water [21] and wax [22] were also embedded in soft robotic systems to generate internal pressures. Soft structures coupled with tendons and driven by electric motors have also been used to develop underactuated and adaptive soft grippers [23], [24].

One of the most common actuation methods employed in soft robotics is pneumatics. There are several types of pneumatic actuators including McKibben actuators [25], fiber-reinforced actuators [26]–[29], and PneuNets [30]–[32] that are activated using positive pressure. Various soft robots and soft structures are designed and actuated based on conventional pneumatic actuators [33]–[40]. There are several manufacturing techniques to fabricate positive pressure actuators, such as molding and additive manufacturing including three-dimensional (3-D) printing based on fused deposition modeling (FDM) [41], [42], stereolithography [43] and multimaterial 3-D printing [44]–[46]. There is also a group of soft pneumatic actuators that uses jamming as a mechanism for conformal gripping [47]. These jamming grippers are activated using a vacuum source instead of a positive pressure source as in conventional soft pneumatic actuators. Various soft pneumatic actuators that are activated using vacuum were recently developed for soft robotic applications [48]–[51]. Soft vacuum actuators have multiple advantages compared to positive pressure actuators. First, the actuators rely on negative pressure which provides a fail-safe feature in contrast to conventional pneumatic actuators where the structure expands upon activation resulting in high stress gradients. Second, vacuum actuators shrink upon activation. This makes them suitable for applications where space requirements are limited. Finally, this actuation method improves the lifetime and durability of the actuators.

All the soft vacuum actuators in the literature [48]–[51] rely on complex manufacturing techniques that require multiple steps to fabricate them [37], [52]. In this article, we propose directly 3-D printed soft actuators that generate a linear motion when activated with negative pressure as shown in Fig. 1 and Movie S1. These linear soft vacuum actuators (LSOVA) have multiple advantages compared to existing soft vacuum actuators. First, they can be easily and rapidly manufactured using an affordable open-source FDM 3-D printer, without requiring any secondary manufacturing process or multiple manufacturing steps. Second, they generate high output forces. The actuators generate a blocked force of 27 N and a lifting force of 26 N upon activation with 95.7% vacuum applied by a pump that can achieve this level of vacuum. Third, the actuators are scalable. The output force increases linearly with an increase in the internal volume of a single actuator. In addition, there is a linear relationship between the output force and the number of actuators connected in parallel to a common output frame. It follows that multiple actuators can be used to amplify the output force for applications requiring a high force. Fourth, the actuators have a high actuation speed. The bandwidth of the LSOVA reported in this study ranges between 3.47 and 6.49 Hz. Fifth, the behavior of the actuators can be accurately predicted using finite element modeling and a geometric model. Sixth, the actuators remain functional, under a continuous supply of vacuum, after failure where their performance is not affected by minor air leaks or structural damage. Finally, the LSOVA can be used in different robotic applications such as soft navigation robots, soft parallel manipulators, soft artificial muscles, soft prosthetics and soft adaptive grippers.

The primary contributions of this article are as follows:

1) propose a linear soft actuation concept based on negative pressure;
2) employ a low-cost and single step 3-D printing technique using an off-the-shelf soft material;
3) quantify the performance of this actuation concept;
4) develop an accurate model to predict its performance; and
5) demonstrate its potential in various soft robotic applications consisting of navigation robots, parallel manipulators, artificial muscles, prosthetics and grippers.

The remainder of this article is organized as follows. Section II presents the fabrication technique, its parameters, and the characteristics of the off-the-shelf printable soft material. Section III presents the finite element modeling of the linear actuation concept and its efficacy in estimating the performance of the actuators and an analytical model that estimates the output blocked force and linear deformation of the LSOVA. The performance of the actuators is comprehensively quantified in terms of step response, hysteresis, bandwidth, blocked force, creep and lifetime in Section IV. Section V presents the results of the scalability experiments. Section VI presents the various robotic applications developed based on LSOVA. Section VII presents the limitations of LSOVA. Finally, section VIII presents conclusions and future work.

II. Materials and Methods

A. Modeling and Fabrication of LSOVA

The actuators were modeled in Autodesk Fusion 360 (Autodesk Inc.). The actuators were designed with 3 mm thick horizontal walls that separate the different vacuum chambers to prevent the structure from collapsing in the lateral direction as shown in Fig. 1(a). Samples were prepared with 1 to 5 vacuum chambers in series and are designated XC-LSOVA with

TABLE I
PERFORMANCE PARAMETERS OF LSOVA

Parameter	1C−LSOVA	2C−LSOVA	3C−LSOVA	4C−LSOVA	5C−LSOVA
L_0	16.00	29.00	42.00	55.00	68.00
V_i	3922.72	7883.13	11843.55	15803.97	19764.40
m	3.16	5.27	7.49	9.46	11.09
δ	6.05	14.58	21.95	28.63	35.03
T_r	60.00	59.00	60.00	64.00	94.00
T_d	631.00	578.00	564.00	570.00	560.00
F_b	27.02	26.56	27.27	27.62	27.66
ω_b	6.49	5.91	5.62	4.69	3.47
L_t	21571	24981	23857	25046	22450

L_0 : Original length (mm), V_i : Internal volume (mm^3), m: Mass (g), δ: Linear deformation (mm), T_r : Rise time (ms), T_d : Decay time (ms), F_b : Blocked force (N), ω_b : Estimated bandwidth (Hz), L_t : Lifetime (cycles).

TABLE II
TPU OPTIMIZED PRINTING PARAMETERS IN SIMPLIFY 3-D

Parameter	Value	Unit
Resolution Settings		
Primary Layer Height	0.1	mm
First Layer Height	0.09	mm
First Layer Width	0.125	mm
Extrusion Width	0.4	mm
Retraction Settings		
Retraction Length	3	mm
Retraction Speed	30	mm/s
Speed Settings		
Default Printing Speed	10	mm/s
Outline Printing Speed	8	mm/s
Solid Infill Speed	8	mm/s
First Layer Speed	8	mm/s
Temperature Settings		
Printing Temperature	240	°C
Heat Bed Temperature	35	°C
Cooling Settings		
Fan Speed	30	%
Infill Settings		
Infill Percentage	100	%
Infill/Perimeter Overlap	20	%
Thin Walls and		
Allowed Perimeter Overlap	15	%
External Thin Wall Type	Perimeters Only	-
Internal Thin Wall Type	Single Extrusion Fill	-
Movements Behavior		
Avoid Crossing Outline	ENABLED	-
Additional Settings		
Extrusion Multiplier	1.15	-
Wipe Nozzle	DISABLED	-
Support Material	DISABLED	-

X representing the number of vacuum chambers in each 3-D printed linear actuator. The dimensions of LSOVA are shown in Fig. 1(a) and given in Table I. The 3-D models were sliced in a commercial 3-D printing software, Simlify3-D (Simplify3-D LLC, OH), where all the printing parameters given in Table II were optimized to obtain airtight actuators. The actuators were printed using an open-source FDM 3-D printer (FlashForge Inventor, USA).

The layer height was set to the minimum value supported by the 3-D printer to obtain airtight actuators and high-quality exteriors. The first layer height and width were adjusted to improve the adhesion of the first layer to the heated bed of the 3-D printer. The first printed layer is very important as it dictates the quality of the overall printed actuator. Therefore, the first layer settings were adjusted to obtain an even and complete first layer. The retraction settings were set to moderate values to avoid any printed plastic residuals. High retraction values lead to underextrusion since the printed thermoplastic polyurethane (TPU) is soft and low values lead to printed plastic residuals. The printing speed was set to a value that ensures continuous and consistent printed lines. High speeds lead to underextrusion as the TPU used is soft. The speed of the first layer was reduced to obtain a complete first layer and the speed of the outermost perimeter was reduced to obtain high quality exteriors. The printing temperature was set to a value that was high enough to ensure that the printed layers were well bonded together to avoid any gaps that might lead to air leaks. The heated bed temperature was set to a value that ensured that the first layer adhered to the bed. A high bed temperature is not desired because it leads to melting the first few printed layers. The cooling speed was set to a moderate value to quickly solidify the printed layers. The cooling load is very critical as the topology of the actuators involves overhangs. The layers should be adequately cooled to avoid any printed layers from sagging. High fan speeds are not recommended as they might lead to moving the printed thin walls and result in shifted layers and consequently air gaps. The infill was set to the maximum value to obtain solid and thick horizontal walls. The perimeter overlap was increased to improve the adhesion and avoid any air gaps between the printed infill and the perimeters. The "avoid crossing outline" option was enabled to ensure that the nozzle does not move over the perimeters where it might leave some plastic residuals that in turn lead to air gaps in the actuators. The extrusion multiplier was increased to account for any inconsistencies in the diameter of the TPU filament.

B. TPU Material Model

A commercially available TPU, known as NinjaFlex (NinjaTek, USA), was used to print the soft actuators. The stress-strain relationship of the TPU was experimentally obtained for use in the finite-element modeling (FEM) and simulations and to understand the behavior of the TPU. Tensile tests were conducted on the TPU according to the ISO 37 standard where the samples were stretched by 800% at a rate of 100 mm/s using an electromechanical Instron Universal Testing machine (Instron8801). Two types of samples were printed using two different infill patterns, crosswise and longitudinal, to assess the effect of the infill on the behavior of the TPU. The samples showed similar behavior which proved that the infill pattern had a minor effect on the behavior of the TPU, as shown in Figs. 2 and 3. The TPU was modeled as a hyperelastic material. The Mooney-Rivlin five-parameter model was identified using the average experimental stress-strain curves of the TPU for both types of infill. The parameters of the hyperelastic material model are given in Table III. The model is implemented in ANSYS Workbench (Release 16.2, ANSYS, Inc.) which provides various hyperelastic material models and curve fitting tools. The material model is used to perform finite element simulations on the soft actuators to predict their quasi-static behavior.

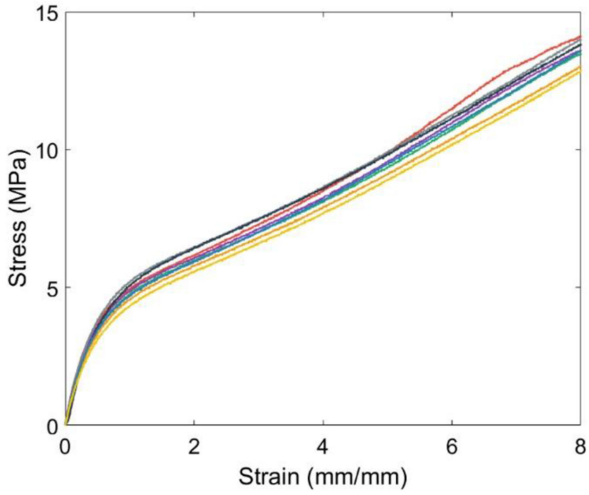

Fig. 2. Experimental stress-strain curves of eight TPU samples printed with a crosswise pattern.

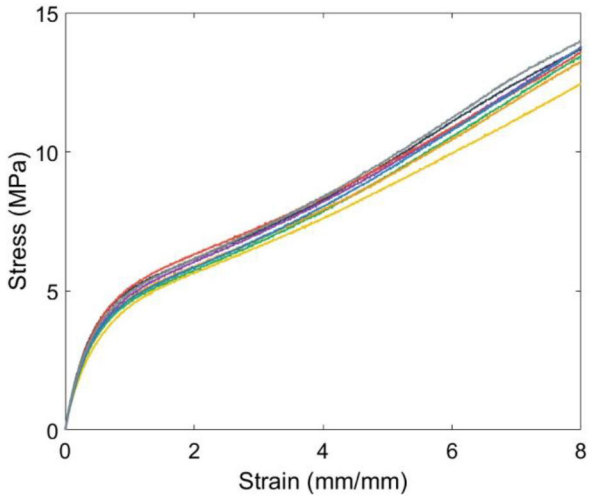

Fig. 3. Experimental stress-strain curves of eight TPU samples printed with a longitudinal pattern.

TABLE III
TPU HYPERELASTIC MATERIAL MODEL CONSTANTS

Hyperelastic Material Model	Material Constant	Value (MPa)
Mooney Rivlin 5-parameter	C10	-0.233
	C01	2.562
	C20	0.116
	C11	-0.561
	C02	0.900
	Incompressibility Parameter D1	0.000

III. MODELING OF LSOVA

A. Finite-Element Modeling

The soft actuators were meshed using higher order tetrahedral elements. Both ends of LSOVA were constrained and a negative pressure was applied on the internal walls. In addition, frictional contact pairs were defined between the internal walls since they touch when the actuators deform. The blocked force and linear deformation of the actuators were predicted using FEM in ANSYS Workbench. The experimental blocked force data matched the FEM results with an acceptable difference of less than 5% in most cases, as given in Table IV. There is a larger discrepancy between the experimental and FEM displacement results, although the FEM did accurately predict the analytical displacement results. The main reason for the discrepancy in the FEM and experimental displacement values was the presence of printing artifacts that reduced the linear displacement. The printed upper horizontal walls of the actuators were not clean and smooth. During the 3-D printing process, the first few layers of each horizontal wall sagged and fell due to the poor bridging performance by NinjaFlex which resulted in thick plastic residuals that interfered with the linear displacement of the LSOVA.

TABLE IV
FINITE-ELEMENT RESULTS FOR LSOVA DEFORMATION AND BLOCKED FORCE

Parameter	1C–LSOVA	2C–LSOVA	3C–LSOVA	4C–LSOVA	5C–LSOVA
δ_e	6.05	14.58	21.95	28.63	35.03
δ_{FEM}	8.65	16.55	23.97	31.94	39.47
$\Delta\delta$	42.98	13.51	9.20	11.56	12.67
$F_{b,\exp}$	27.02	26.56	27.27	27.62	27.66
$F_{b,\mathrm{FEM}}$	28.30	28.49	28.59	28.56	28.66
ΔF_b	4.72	7.26	4.85	3.39	3.62

δ_e: Experimental deformation (mm), δ_{FEM} : FEM deformation (mm), $F_{b,\exp}$: Experimental blocked force (N), $F_{b,\mathrm{FEM}}$: FEM blocked force (N), $\Delta\delta$: Difference between δ_e and δ_{FEM} (%), ΔF_b : Difference between $F_{b,\exp}$ and $F_{b,\mathrm{FEM}}$ (%)

To verify this hypothesis, a 1C–LSOVA was cut in half and its interior walls were cleaned. Then, the cleaned 1C–LSOVA was glued back together and its displacement was measured upon activation with 95.7% vacuum. The actuator displacement increased from 6.05 to 8.57 mm which resulted in a difference of 0.93% when compared to the FEM. During the blocked force experiment, the walls of LSOVA remained undeformed since the actuators were restricted from moving which resulted in very accurate blocked force results.

The maximum and minimum running times of the FEM simulations for the 20 mm diameter LSOVA are 969 and 83 s, respectively. The LSOVA with more chambers required more computational time compared to shorter LSOVA since the mesh size increases with the number of chambers. However, it is important to note that the simulation time can be significantly decreased by allocating more memory. The only challenge encountered was the distortion of some elements due to the large mechanical deformations. However, this issue was alleviated by incorporating a coarser mesh that is suitable for hyperelastic materials. The mesh used was selected to verify that the results are accurate and not affected by the mesh size. Therefore, FEM can be used to optimize the performance of LSOVA rapidly and efficiently. The performance of the reported soft vacuum actuators in [48]–[51] was predicted either by experimental data

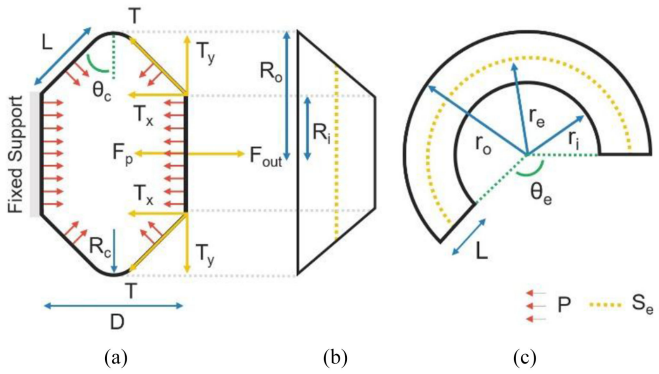

Fig. 4. FBD. (a) LSOVA FBD. (b) Frustum side view. (c) Flattened frustum.

TABLE V
1C–LSOVA ANALYTICAL MODEL PARAMETERS

Parameter	Value
F_{out}	28.97
F_p	24.05
T_x	4.92
P	98.19
R_i	8.83
R_o	12.87
R_c	0.50
r_i	14.04
r_o	20.47
r_e	17.05
L	6.43
S_e	67.35
D	9.85
θ_c	50.00
θ_e	226.35

F_{out}: Output force (N), F_p: Pressure force (N), T_x: Thin wall horizontal tension (N), P: Input negative pressure (kPa), R_i: LSOVA inner radius (mm), R_o: LSOVA outer radius (mm), R_c: Radius of curvature (mm), r_i: Flattened frustum inner radius (mm), r_o: Flattened frustum outer radius (mm), r_e: Flattened frustum effective radius (mm), L: Thin Wall Length (mm), S_e: Thin wall width (mm), D: Linear stroke (mm), θ_c: LSOVA angle (°), θ_e Frustum effective angle (°).

solely, empirical models or analytical models. Finally, we have employed the FEM to analyze and size of the actuators evaluated in the remainder of this article.

B. Analytical Model

We derived an analytical model to estimate the blocked force of the actuators. The free-body diagram (FBD) of a 1C–LSOVA is shown in Fig. 4 and all the parameters of the model are given in Table V.

The output blocked force can be expressed as

$$F_{\text{out}} = F_p + 2T_x \tag{1}$$

where

$$F_p = \pi R_i^2 P. \tag{2}$$

From Laplace's law, we can write

$$T = R_c P S_e \tag{3}$$

where S_e is the effective width of the thin walls which was computed by considering the flattened frustum shown in Fig. 4(c).

The relationship between LSOVA inner and outer radii and the flattened frustum inner and outer radii can be expressed as follows:

$$r_i = R_i L/(R_o - R_i) \tag{4}$$

$$r_o = R_o L/(R_o - R_i) \tag{5}$$

and the effective radius of the flattened frustum can be computed from the following equation:

$$r_e = L/\ln(r_o/r_i). \tag{6}$$

The effective length of the frustum can be now computed as follows:

$$S_e = r_e \theta_e \tag{7}$$

where

$$\theta_e = (R_o - R_i)/L \tag{8}$$

The horizontal component of the tension can now be written as follows:

$$T_x = T\sin\theta_c = R_c P S_e \sin\theta_c. \tag{9}$$

Finally, the output blocked force becomes

$$F_{\text{out}} = P\left(\pi R_i^2 + 2R_c S_e \sin\theta_c\right). \tag{10}$$

Using the data in Table V and comparing with the experimental blocking force in Table IV for 1C–LSOVA, the difference between the experimental and analytical blocked force for 1C–LSOVA is 7.20%. This follows that the analytical model can be used to predict the blocked force of LSOVA with reasonable accuracy. The main difference between the analytical and experimental blocked forces can be attributed to the fact that the analytical model does not consider the mechanical properties of the TPU used. The analytical model assumes that the walls are rigid and behave like rigid links. Therefore, the experimental blocked force is less compared to the analytical blocked force due to the softness of the TPU used to 3-D print the soft actuators

From Fig. 4, we can find the relationship between the linear stroke (D) and the angle θ_c, by assuming that the walls are undeformable, which can be written as follows:

$$D = 2L\sin\theta_c. \tag{11}$$

The difference between the predicted linear stroke by the analytical model and the experimental linear stroke of 8.57 mm is 14.94% which is reasonable considering that the real deformation is limited by the thick plastic residuals (i.e., printing artifacts) that interfered with the linear displacement of the LSOVA, as explained earlier. This proves that the analytical model is effective enough to estimate the blocked force and output linear stroke of the LSOVA.

IV. LSOVA CHARACTERIZATION

A. Step Response

The step responses of five linear actuators that consist of multiple number of vacuum chambers were obtained using a

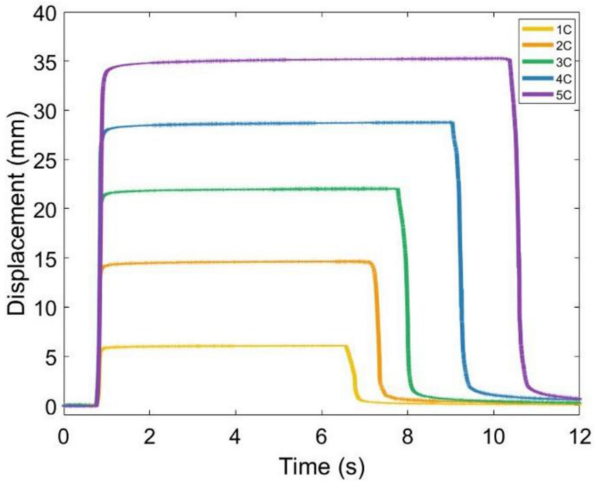

Fig. 5. Step response curves of various LSOVA consisting of different numbers of vacuum chambers.

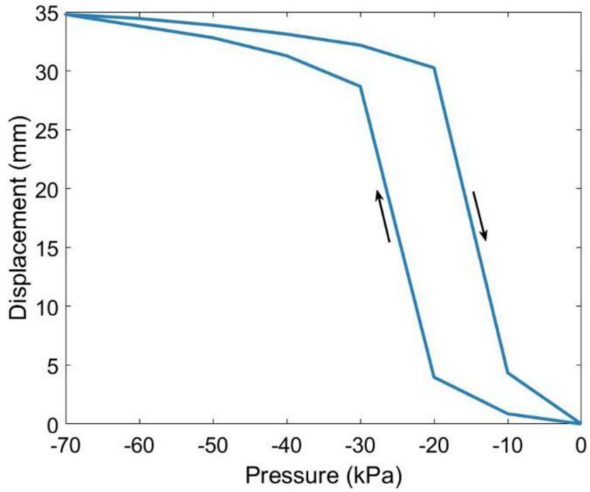

Fig. 6. Hysteresis curve of a 5C–LSOVA.

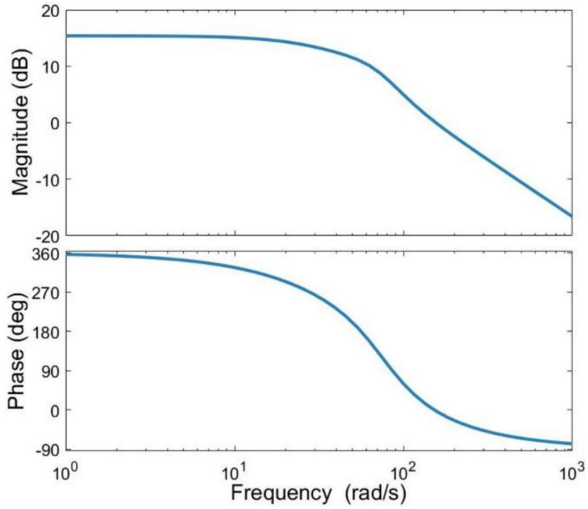

Fig. 7. Bode plot for 1C–LSOVA.

high-resolution laser sensor (Micro-Epsilon, optoNCDT 1700-50) that measured their linear displacement upon activation with 95.7% vacuum. As shown in Fig. 5, the actuators responded rapidly when vacuum was applied and recovered their initial position quickly when their internal pressure was returned to the atmospheric pressure using a solenoid valve (12VDC solenoid valve, air leakage 1cc/min). The rise time and decay time of each LSOVA are given in Table I. The rise time of LSOVA is 25 times less than the rise time reported in [49], at least three times less than the rise time reported in [50] and eight times less than the rise time reported in [51]. The rise time of LSOVA increased with the number of vacuum chambers. Also, the decay times of LSOVA were larger compared to their rise times since the actuators internal pressure was returned to atmospheric pressure using a solenoid valve and consequently the actuators were not forced to recover their initial position. In addition, the buckling of the thin walls affected the recovery speed of LSOVA. The thin walls did not recover their initial shape directly upon activation of the solenoid valve. The linear stroke of the actuators changed drastically after the vacuum pressure reached $P = -20$ kPa as shown in Fig. 6.

B. Hysteresis

The linear displacement of a 5C–LSOVA was measured when the input negative pressure was ramped up and down by a step of $\Delta P = -10$ kPa. The actuator exhibited hysteresis with the largest difference of 26.27 mm occurring at $P = -20$ kPa as shown in Fig. 6. The buckling of the thin walls upon activation is the main reason for the hysteresis. The actuator contracts rapidly after the internal pressure reaches $P = -20$ kPa.

C. Actuation Frequencies and Bandwidths

The maximum actuation frequency (i.e., bandwidth) of LSOVA was obtained by activating the structure with 95.7% vacuum. The experimental actuation frequencies were limited by the speed of the solenoid valves and the inconsistent rate of discharge of the vacuum pump at high frequencies. Consequently, higher actuation frequencies were not achieved due to the limitations imposed by the pneumatic equipment. The actuation frequency decreased with an increase in the number of vacuum chambers. This is mainly because the actuators with a high number of cells have a larger internal volume to evacuate, and subsequently, more time is needed to fill them with air at the atmospheric pressure. This process will naturally increase the response time (in other words decrease the bandwidth) of the actuators. The bandwidths of the distinct LSOVAs were estimated from their experimental step responses (see Fig. 5), from which the corresponding Bode plots (e.g., Figs. 7 and 8) were obtained for 1C–LSOVA and 5C–LSOVA. The bandwidths of LSOVA are given in Table I. The bandwidth of a 1C–LSOVA is 32 times greater than the bandwidth reported in [48] and 5.9 times greater than the bandwidth reported in [49]. The bandwidths of the other soft vacuum actuators in [50] and [51] are not reported. Similarly, the bandwidth of a 5C–LSOVA

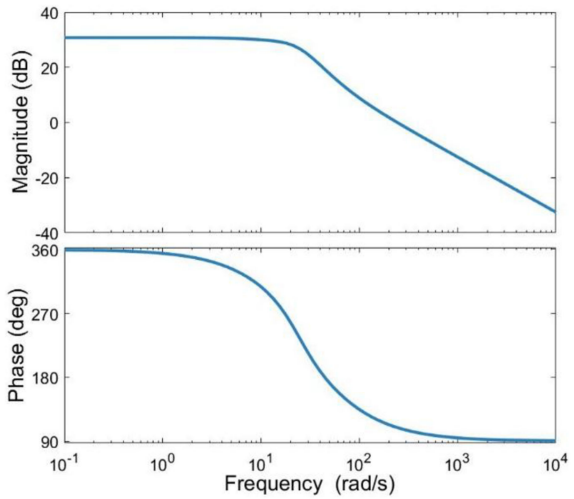

Fig. 8. Bode plot for 5C–LSOVA.

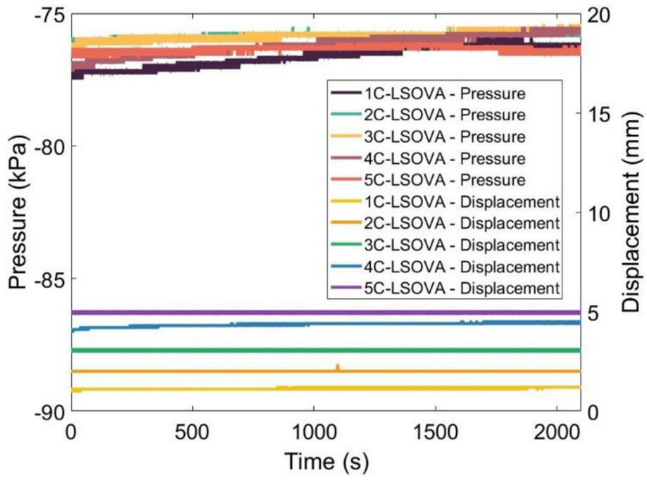

Fig. 9. Creep experiment. Pressure and displacement (the bottom curves) curves of LSOVA.

is 17 times greater than the bandwidth reported in [48] and 3.5 times greater than the bandwidth reported in [49]. The design and material properties of the LSOVA contributed to their high bandwidths. First, the design of the thick horizontal walls and the thin walls allow a single chamber to quickly collapse in the vertical direction under negative pressure. Also, since NinjaFlex is soft but not stretchable, a single chamber is quickly deformed without any loss in energy due to the softness of the material.

D. Blocked Force

The blocked force of the actuators was measured using a force gauge (5000 g, FG-5005, Lutron Electronic Enterprise CO., LTD). The actuators were restricted from moving by constraining both ends when 95.7% vacuum was applied to measure the blocked force. The forces generated by various actuators consisting of a different number of vacuum chambers are given in Table I. The blocked force reported in [49] varied between 90 and 428 N based on various designs. The blocked force produced by LSOVA is lower compared to the blocked force reported in [49]. However, it is important to note that a 30 mm diameter LSOVA generated a blocked force of 60.58 N as presented in Section V about LSOVA scalability. Therefore, LSOVA can be scaled up to produce higher output forces. In [50], two types of soft vacuum linear actuators with different material properties were reported where the blocked force of a 20 mm diameter LSOVA is eight times larger than the blocked force of the first actuator reported and comparable with the blocked force of the second actuator reported. Similarly, the blocked force of a 20 mm diameter LSOVA is 68 times larger compared to the blocked force of the first design reported in [51] and 30 times larger compared to the blocked force of the second design reported. The blocked force of LSOVA was larger compared to soft vacuum actuators made of softer materials. Although NinjaFlex is soft, it cannot stretch as silicone. This property enhanced the blocked force and payload of LSOVA. The output force was consistent for the various linear actuators. The experimental and FEM results showed that the output blocked force in not dependent on the length of the actuators. To explain this consistency in the blocked force we refer to the FBD, as shown in Fig. 4. By taking a section cut on the first cell of a 5C–LSOVA, the output blocked force is equal to the internal force at this section. In fact, this internal force is equal to the output force of a 1C–LSOVA since an equilibrium of forces in the horizontal direction must be satisfied. Therefore, long actuators can be used without affecting the output force to target applications where large linear strokes are desired or required.

E. Creep

The internal pressure of the actuators was kept constant for a period of 35 min while their position was monitored to detect any drift resulting from creep. The actuators experienced no creep as shown in Fig. 9, which confirms that creep is independent of the number of cells. The position of the actuators remained unchanged during the activation period. The pressure of the system changed slightly by 0.32% for the longest actuator during the experiment, causing a negligible change in the actuator stroke, due to minor air leakage from fittings and connectors.

F. Lifetime and Durability

The number of cycles that the actuators sustained before failure was measured by activating them using 90% vacuum generated by a vacuum pump (Gardner Denver Thomas GmbH). It must be noted that the vacuum pump used in the previous experimental results could generate up to 95.7% vacuum. However, this pump was not practical and powerful enough to apply multiple thousands of cycles of the same vacuum. Therefore, we used this more powerful vacuum pump to apply 90% vacuum for the lifetime and durability experiments. In each actuation cycle, the actuators were activated to achieve full contraction. The LSOVA performance remained unchanged prior to failure. The internal pressure of LSOVA was returned to atmospheric in each cycle to recover their initial position after they were

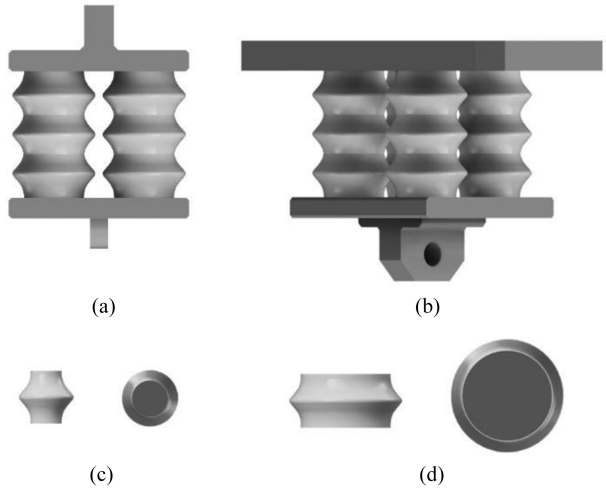

Fig. 10. LSOVA output force amplification. (a) Bundle of two 3C–LSOVA. (b) Bundle of four 3C–LSOVA. (c) 1C–LSOVA with a diameter of 10 mm, an area of 591 mm^2 and a volume of 1226 mm^3 . (d) 1C–LSOVA with a diameter of 30 mm, an area of 2514 mm^2 and a volume of 8191 mm^3. The area of a 20 mm diameter 1C–LSOVA is 1396 mm^2.

fully contracted. The lifetimes of the actuators are given in Table I. The lifetime of LSOVA is significantly higher compared to the reported lifetime of other 3-D printed soft actuators [41], [43]. The main reason for the failure was the separation of the layers at the edges where the actuator cells experience high stress concentrations. It was observed that thicker walls result in high stress gradients at the edges of LSOVA upon activation. Even though the actuators failed, they were still able to lift the same load under a continuous supply of vacuum. It follows that they are fault-tolerant during operation. The main reason that these actuators are fault-tolerant is that the pressure loss due to the air gaps created after failure can be compensated by a continuous vacuum supply. Also, the contraction of the actuator walls upon activation blocks the air gaps created. An airtight 1C–LSOVA with thinner walls (0.55 mm) was tested and was able to sustain 80 000 actuation cycles prior to failure which was approximately four times the lifetime of an LSOVA with thicker walls (0.68 mm). The effect of the wall thickness on the performance of LSOVA is discussed in Section VII.

V. Scalability

One of the advantages of the LSOVA is to assemble them in parallel to generate high output forces. There is a linear relationship between the number of actuators and the output force generated. Although the actuators are soft, high output forces and large linear displacements can be generated by implementing them as a bundle of linear actuators as shown in Fig. 10 and Movie S2. A bundle of two and four 3C–LSOVA can lift 5.0 and 10.0 kg, respectively when activated with 95.7% vacuum. In addition, the output force increases linearly with an increase in the internal volume of a single actuator for the same vacuum pressure (see Fig. 10). A 10 mm diameter 1C–LSOVA generated a blocked force of 6.86 N and lifted a maximum load of 0.6 kg when activated with 95.7% vacuum (see Fig. 10). Similarly, a 30 mm diameter 1C–LSOVA generated a blocked force of 60.58 N and lifted a maximum load of 5.1 kg. Using (10) from the analytical model, we have obtained a blocked force of 7.16 N for a 10 mm diameter LSOVA with a difference of 4.42% compared to the experimental blocked force of 6.86 N. Similarly, we have obtained a blocked force of 66.41 N for a 30 mm diameter LSOVA with a difference of 8.77% compared to the experimental blocked force of 60.59 N.

Therefore, the area of a single actuator can be chosen depending on the output force required for a specific application. The scalability of the actuators presented in [49] is challenging as reported since the actuators are composed of a soft skin and an internal skeleton. The performance of these scaled actuators was experimentally obtained. Also, the reported actuators in [50] and [51] are scalable. However, they should be carefully fabricated to obtain specific material properties that lead to the desired performance as opposed to LSOVA which can directly be scaled up or down using 3-D printing. Moreover, the performance of the scaled LSOVA can be accurately predicted using the FEM and analytical models prior to fabrication. However, it is important to note that since NinjaFlex has a poor bridging performance during the 3-D printing process, the surface area cannot be increased dramatically.

VI. Applications

LSOVA can be tailored to various robotic applications where they can be implemented as soft actuators.

A. Crawling Robot in Transparent Plastic Tube

We developed a crawling robot that moved through plastic tubes as shown in Fig. 11 and Movie S3. The robot is composed of three separate LSOVAs. The ends of the robot are designed carefully to push against the wall of the tube upon activation to hold it in place while the middle section of the robot moves it in the desired direction. The total body length of the robot is 70.5 mm. Both ends of the robot are made of a 20 mm diameter 1C–LSOVA while the middle section is made of a 15 mm diameter 2C–LSOVA. The robot moved with average horizontal and vertical speeds of 1.26 and 1.11 mm/s, respectively, upon activation with 95.7% vacuum. The robot can move forward and backward depending on the actuation sequence imposed.

B. Soft Manipulator With Vacuum Suction Cup

We developed a parallel soft manipulator based on 3C–LSOVA as shown in Fig. 11 and Movie S4. The manipulator can reach a bending angle of 90° when one of the parallel connected actuators is activated using 95.7% vacuum. At the tip of the manipulator, we attached a 3-D printed suction cup to show the versatility of LSOVAs. The soft manipulator could move to eight various positions while picking and placing objects. Here, we demonstrated that the soft manipulator was capable of picking carton pieces and placing them in different containers. In addition, the manipulator was capable of lifting and manipulating a maximum load of 0.5 kg. This kind of soft

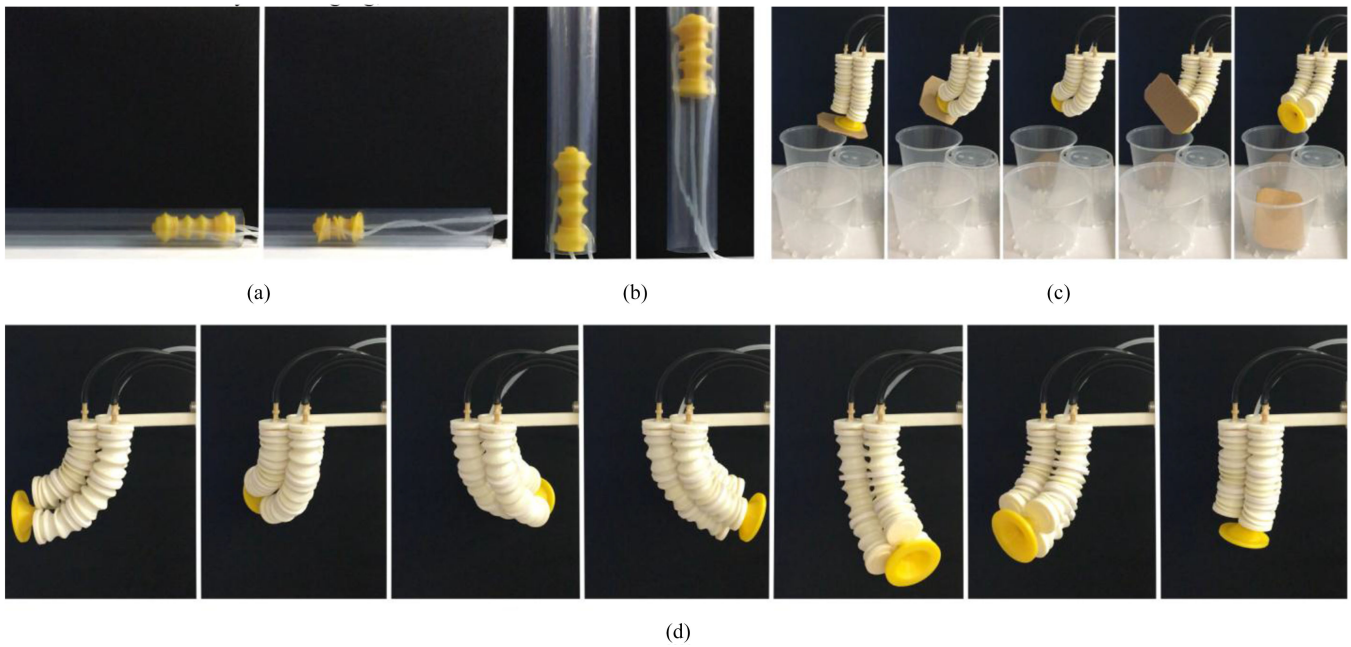

Fig. 11. Applications of LSOVA. Images of crawling robot in a smooth and transparent 32mm diameter vinyl tube. (a) Horizontal tube (Left: Initial Position, Right Final Position). (b) Vertical tube. (c) Parallel manipulator picking and placing carton pieces in two different containers. (d) Parallel manipulator in seven distinct positions. The remaining position where none of the actuators is activated is not shown.

manipulators can be used in industrial applications on assembly and sorting lines to pick and place delicate structures with moderate weights. This kind of manipulators can interact safely with their environment since they are made of soft materials.

C. Soft Artificial Muscle

A single or multiple LSOVAs can be used as soft artificial muscles that can generate high forces. In this scenario, we implemented a 5C–LSOVA actuator to move an elbow joint by an angle of 45°, as shown in Fig. 12 and Movie S5. The artificial muscle can lift a maximum load of 0.5 kg. When no load was imposed on the system, the palm of the hand moved vertically upward by 130 mm. However, when the system was loaded with a 0.5 kg mass, the vertical distance decreased to 115 mm.

D. Soft Prosthetic Fingers and Grippers

Using the same 3-D printing technique in [23] and [53]–[56], we fabricated a monolithic body with flexural joints, so that it could be configured as a soft prosthetic finger when activated using one 5C–LSOVA coupled with a tendon. The actuator pulled the tendon upon activation with 95.7% vacuum causing the prosthetic finger to bend as shown in Fig. 12 and Movie S6. The LSOVA actuators can be coupled with tendons for soft prosthetic applications requiring a high force. The soft prosthetic finger can grasp various objects as shown in Fig. 12. In addition, we have 3-D printed a soft gripper based on these three soft fingers. The gripper was driven by one 5C–LSOVA coupled with tendons that run through the soft finger. The gripper lifted a load of 1.0 kg. The load capacity of the soft gripper was highly dependent on the design of the fingers. In this scenario, the geometry of the fingers was not optimized, but used only for demonstration purpose. Also, since the gripper is compliant, it can grasp and interact safely with flexible objects as shown in Fig. 12 and Movie S7.

VII. Discussion

One main downside of LSOVA is the nonlinear relationship between the input negative pressure and the stroke (i.e., displacement) of the actuator, as shown in Fig. 6. The walls of the actuators buckle after a certain level of vacuum which causes a rapid deformation. We postulate that the main reason behind the large hysteresis exhibited by LSOVA is the buckling of the thin walls. This nonlinear behavior makes the control of LSOVA very challenging, which is one of the future research topics. The objective of this article is to directly 3-D print or fabricate low-cost and airtight linear soft actuators that can be activated through vacuum. The soft actuators developed were not comprehensively optimized to operate at their maximum performance. The geometry of the actuators greatly affects their performance in terms of blocked force, lifting force, rectilinear displacement, actuation frequency, and lifetime. The wall thickness of LSOVAs is the main parameter that needs to be optimized. It was proved experimentally that actuators with thinner walls had a higher output force, higher lifting force, longer lifetime and higher payload-to-weight ratio. However, airtightness becomes a major concern when printing soft actuators with thin walls. Therefore, the thickness of the walls should be optimized to ensure airtightness and maximum possible performance. In addition, only circular shapes were considered in this article. However, LSOVA can be printed in different shapes, such as

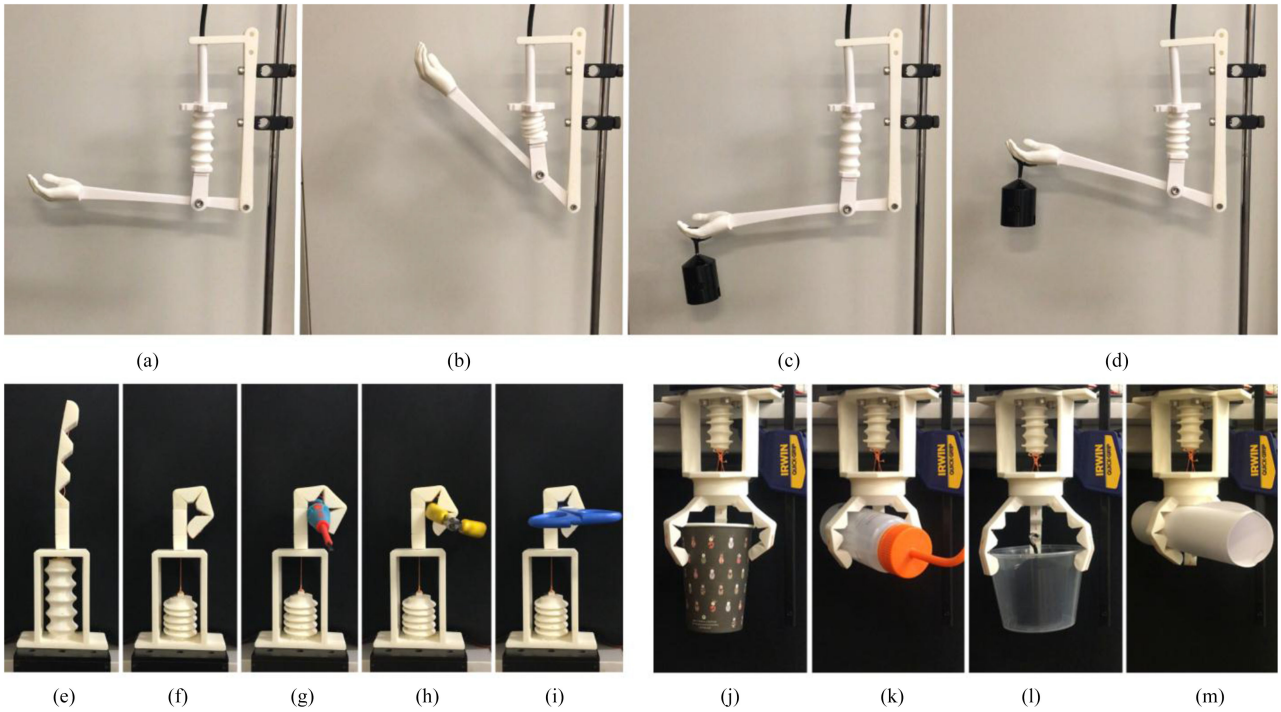

Fig. 12. Practical applications of LSOVA. Elbow joint. (a) Unloaded. (b) Unloaded and activated with 95.7% vacuum. (c) Loaded with a 0.5 kg weight and not activated. (d) Loaded with a 0.5 kg weight and activated with 95.7% vacuum. Soft finger. (e) Open position and (f) closed position. Soft finger grasping (g) a screwdriver (21.61 g), (h) a plier (54.35 g), and (i) scissors (30.58 g) upon activation with 95.7% vacuum. Soft gripper grasping (j) a cup (11.32 g), (k) a bottle (45.94 g), (j) a plastic container (1000 g), and (m) a flexible paper cylinder (4.95 g) upon activation with 95.7% vacuum.

rectangular and elliptical with various aspect ratios to target specific applications.

VIII. Conclusion and Future Work

In this article, we have established 3-D printable linear soft actuators, LSOVA, that can be activated through vacuum. The actuators were directly manufactured using a low-cost open-source FDM 3-D printer, without requiring any secondary manufacturing or assembly process. The vacuum actuators generate high output forces and large rectilinear displacements.

In addition, the quasi-static behavior of LSOVA can be accurately predicted in terms of the linear displacement and blocked force using FEM and a geometric model. The actuators presented in this article can be optimized to achieve maximum performance. The wall thickness of the actuators affects their performance. In future studies, the wall thickness of LSOVA will be optimized to achieve maximum performance while preserving airtightness. In addition, LSOVA will be designed using several geometrical shapes including rectangular and elliptical cross-sections with various aspect ratios. We have demonstrated the potential of these actuators for employment in various robotic applications, such as navigation robots, robotic manipulators artificial muscles, prosthetics, and grippers.

Acknowledgment

The authors would like to thank Dr. R. Mutlu (University of Wollongong) for assistance with 3-D printing of the actuators.

References

[1] B. Trimmer, "Soft robots," *Current Biol.*, vol. 23, no. 15, pp. R639–R641, 2013.
[2] D. Rus and M. T. Tolley, "Design, fabrication and control of soft robots," *Nature*, vol. 521, pp. 467–475, 2015.
[3] D. Trivedi, C. D. Rahn, W. M. Kier, and I. D. Walker, "Soft Robotics: Biological inspiration, state of the art, and future research," *Appl. Bionics Biomech.*, vol. 5, no. 3, 2008.
[4] L. Huai-Ti, G. L. Gary, and T. Barry, "GoQBot: A caterpillar-inspired soft-bodied rolling robot," *Bioinspiration Biomimetics*, vol. 6, no. 2, p. 026007, 2011.
[5] C. Laschi, M. Cianchetti, B. Mazzolai, L. Margheri, M. Follador, and P. Dario, "Soft robot arm inspired by the octopus," *Adv. Robot.*, vol. 26, no. 7, pp. 709–727, 2012.
[6] J. Hu, D. Erbao, X. Min, L. Chunshan, G. Alici, and J. Yang, "Soft and smart modular structures actuated by shape memory alloy (SMA) wires as tentacles of soft robots," *Smart Mater. Struct.*, vol. 25, no. 8, 2016, Art. no. 085026.
[7] Y. She, C. Li, J. Cleary, and H.-J. Su, "Design and fabrication of a soft robotic hand with embedded actuators and sensors," *J. Mechanisms Robot.*, vol. 7, no. 2, pp. 021007–021007-9, 2015.
[8] S. Seok, C. D. Onal, K. J. Cho, R. J. Wood, D. Rus, and S. Kim, "Meshworm: A peristaltic soft robot with antagonistic nickel titanium coil actuators," *IEEE/ASME Trans. Mechatronics*, vol. 18, no. 5, pp. 1485–1497, Oct. 2013.
[9] G. Guo-Ying, Z. Jian, Z. Li-Min, and Z. Xiangyang, "A survey on dielectric elastomer actuators for soft robots," *Bioinspiration Biomimetics*, vol. 12, no. 1, p. 011003, 2017.
[10] N. Kellaris, V. Gopaluni Venkata, G. M. Smith, S. K. Mitchell, and C. Keplinger, "Peano-HASEL actuators: Muscle-mimetic, electrohydraulic transducers that linearly contract on activation," *Sci. Robot.*, vol. 3, no. 14, p. aar3276, 2018.
[11] B. Yousef and S. Mohsen, "A review of ionic polymeric soft actuators and sensors," *Soft Robot.*, vol. 1, no. 1, pp. 38–52, 2014.
[12] C. S. Haines *et al.*, "Artificial muscles from fishing line and sewing thread," *Science*, vol. 343, no. 6173, pp. 868–872, 2014.

[13] G. M. Spinks, "Stretchable artificial muscles from coiled polymer fibers," *J. Mater. Res.*, vol. 31, no. 19, pp. 2917–2927, 2016.
[14] S. E. Bakarich, R. Gorkin, M. I. H. Panhuis, and G. M. Spinks, "4D printing with mechanically robust, thermally actuating hydrogels," *Macromol. Rapid Commun.*, vol. 36, no. 12, pp. 1211–1217, 2015.
[15] H. Yuk, S. Lin, C. Ma, M. Takaffoli, N. X. Fang, and X. Zhao, "Hydraulic hydrogel actuators and robots optically and sonically camouflaged in water," *Nat. Commun.*, vol. 8, 2017, Art. no. 14230.
[16] B. Shin *et al.*, "Hygrobot: A self-locomotive ratcheted actuator powered by environmental humidity," *Sci. Robot.*, vol. 3, no. 14, p. aar2629, 2018.
[17] W. Hu, G. Z. Lum, M. Mastrangeli, and M. Sitti, "Small-scale soft-bodied robot with multimodal locomotion," *Nature*, vol. 554, pp. 81–85, 2018.
[18] N. W. Bartlett *et al.*, "A 3D-printed, functionally graded soft robot powered by combustion," *Science*, vol. 349, no. 6244, pp. 161–165, 2015.
[19] K. Suzumori, A. Wada, and S. Wakimoto, "New mobile pressure control system for pneumatic actuators, using reversible chemical reactions of water," *Sens. Actuators, A*, vol. 201, pp. 148–153, 2013.
[20] M. Wehner *et al.*, "An integrated design and fabrication strategy for entirely soft, autonomous robots," *Nature*, vol. 536, pp. 451–466, 2016.
[21] A. Miriyev, K. Stack, and H. Lipson, "Soft material for soft actuators," *Nature Commun.*, vol. 8, no. 1, 2017, Art. no. 596.
[22] J. I. Lipton, S. Angle, R. E. Banai, E. Peretz, and H. Lipson, "Electrically actuated hydraulic solids," *Adv. Eng. Mater*, vol. 18, no. 10, pp. 1710–1715, 2016.
[23] R. Mutlu, G. Alici, M. in het Panhuis, and G. Spinks, "3D printed flexure hinges for soft monolithic prosthetic fingers," *Soft Robot.*, vol. 3, no. 3, pp. 120–133, 2016.
[24] M. Manti, T. Hassan, G. Passetti, N. D'Elia, C. Laschi, and M. Cianchetti, "A bioinspired soft robotic gripper for adaptable and effective grasping," *Soft Robot.*, vol. 2, no. 3, pp. 107–116, 2015.
[25] C. Ching-Ping and B. Hannaford, "Measurement and modeling of McKibben pneumatic artificial muscles," *IEEE Trans. Robot. Automat.*, vol. 12, no. 1, pp. 90–102, Feb. 1996.
[26] K. C. Galloway, P. Polygerinos, C. J. Walsh, and R. J. Wood, "Mechanically programmable bend radius for fiber-reinforced soft actuators," in *Proc. Int. Conf. Adv. Robot.*, 2013, pp. 1–6.
[27] F. Connolly, P. Polygerinos, C. J. Walsh, and K. Bertoldi, "Mechanical programming of soft actuators by varying fiber angle," *Soft Robot.*, vol. 2, no. 1, pp. 26–32, 2015.
[28] M. Robertson, H. Sadeghi, J. Florez, and J. Paik, "Soft pneumatic actuator fascicles for high force and reliability," *Soft Robot.*, vol. 4, no. 1, pp. 23–32, 2017.
[29] S. Nikolov, V. Kotev, K. Kostadinov, F. Wang, C. Liang, and Y. Tian, "Model-based design optimization of soft fiber-reinforced bending actuators," in *Proc. IEEE Int. Conf. Manipulation, Manuf. Meas. Nanoscale*, 2016, pp. 136–140.
[30] O. Keiko, S. Wakimoto, K. Suzumori, and N. Yasutaka, "Micro pneumatic curling actuator - nematode actuator," in *Proc. IEEE Int. Conf. Robot. Biomimetics.*, 2009, pp. 462–467.
[31] G. Alici, T. Canty, R. Mutlu, W. Hu, and V. Sencadas, "Modeling and experimental evaluation of bending behavior of soft pneumatic actuators made of discrete actuation chambers," *Soft Robot.*, vol. 5, no. 1, pp. 24–35, 2018.
[32] B. Mosadegh *et al.*, "Pneumatic networks for soft robotics that actuate rapidly," *Adv. Funct. Mater*, vol. 24, no. 15, pp. 2163–2170, 2014.
[33] S. Terryn, J. Brancart, D. Lefeber, G. Van Assche, and B. Vanderborght, "Self-healing soft pneumatic robots," *Sci. Robot.*, vol. 2, no. 9, p. aan4268, 2017.
[34] E. W. Hawkes, L. H. Blumenschein, J. D. Greer, and A. M. Okamura, "A soft robot that navigates its environment through growth," *Sci. Robot.*, vol. 2, no. 8, p. aan3028, 2017.
[35] J. D. Greer, T. K. Morimoto, A. M. Okamura, and E. W. Hawkes, "Series pneumatic artificial muscles (sPAMs) and application to a soft continuum robot," in *Proc. IEEE Int. Conf. Robot. Automat.*, 2017, pp. 5503–5510.
[36] R. V. Martinez, C. R. Fish, X. Chen, and G. M. Whitesides, "Elastomeric origami: programmable paper-elastomer composites as pneumatic actuators," *Adv. Funct. Mater*, vol. 22, no. 7, pp. 1376–1384, 2012.
[37] A. Argiolas *et al.*, "Sculpting soft machines," *Soft Robot.*, vol. 3, no. 3, pp. 101–108, 2016.
[38] E. W. Hawkes, D. L. Christensen, and A. M. Okamura, "Design and implementation of a 300% strain soft artificial muscle," in *Proc. IEEE Int. Conf. Robot. Automat.*, 2016, pp. 4022–4029.
[39] R. Niiyama, X. Sun, C. Sung, B. An, D. Rus, and S. Kim, "Pouch motors: Printable soft actuators integrated with computational design," *Soft Robot.*, vol. 2, no. 2, pp. 59–70, 2015.
[40] R. V. Martinez, A. C. Glavan, C. Keplinger, A. I. Oyetibo, and G. M. Whitesides, "Soft actuators and robots that are resistant to mechanical damage," *Adv. Funct. Mater*, vol. 24, no. 20, pp. 3003–3010, 2014.
[41] H. K. Yap, H. Y. Ng, and C.-H. Yeow, "High-force soft printable pneumatics for soft robotic applications," *Soft Robot.*, vol. 3, no. 3, pp. 144–158, 2016.
[42] B. A. W. Keong and R. Y. C. Hua, "A novel fold-based design approach toward printable soft robotics using flexible 3D printing materials," *Adv. Mater. Technol.*, vol. 3, no. 2, p. 1700172, 2018.
[43] N. P. Bryan, J. W. Thomas, Z. Huichan, and F. S. Robert, "3D printing antagonistic systems of artificial muscle using projection stereolithography," *Bioinspiration Biomimetics*, vol. 10, no. 5, 2015, Art. no. 055003.
[44] R. MacCurdy, R. Katzschmann, K. Youbin, and D. Rus, "Printable hydraulics: A method for fabricating robots by 3D co-printing solids and liquids," in *Proc. IEEE Int. Conf. Robot. Automat.*, 2016, pp. 3878–3885.
[45] M. Schaffner, J. A. Faber, L. Pianegonda, P. A. Rühs, F. Coulter, and A. R. Studart, "3D printing of robotic soft actuators with programmable bioinspired architectures," *Nat. Commun.*, vol. 9, no. 1, 2018, Art. no. 878.
[46] T. Kalisky *et al.*, "Differential pressure control of 3D printed soft fluidic actuators," in *Proc. IEEE/RSJ Int. Conf. Intell. Robot. Syst.*, 2017, pp. 6207–6213.
[47] E. Brown *et al.*, "Universal robotic gripper based on the jamming of granular material," *Proc. Nat. Acad. Sci.*, vol. 107, no. 44, pp. 18809–18814, 2010.
[48] M. A. Robertson and J. Paik, "New soft robots really suck: Vacuum-powered systems empower diverse capabilities," *Sci. Robot.*, vol. 2, no. 9, p. aan6357, 2017.
[49] S. Li, D. M. Vogt, D. Rus, and R. J. Wood, "Fluid-driven origami-inspired artificial muscles," *Proc. Nat. Acad. Sci.*, vol. 114, no. 50, pp. 13132–13137, 2017.
[50] D. Yang *et al.*, "Buckling pneumatic linear actuators inspired by muscle," *Adv. Mater. Technol.*, vol. 1, no. 3, 2016, Art. no. 1600055.
[51] D. Yang, M. S. Verma, E. Lossner, D. Stothers, and G. M. Whitesides, "Negative-pressure soft linear actuator with a mechanical advantage," *Adv. Mater. Technol.*, vol. 2, no. 1, 2017, Art. no. 1600164.
[52] A. D. Marchese, R. K. Katzschmann, and D. Rus, "A recipe for soft fluidic elastomer robots," *Soft Robot.*, vol. 2, no. 1, pp. 7–25, 2015.
[53] C. Tawk, M. in het Panhuis, G. M. Spinks, and G. Alici, "Bioinspired 3D printable soft vacuum actuators (SOVA) for locomotion robots, grippers and artificial muscles," *Soft Robot.*, vol. 5, no. 6, pp. 685–694, 2018.
[54] C. Tawk, A. Gillett, M. in het Panhuis, G. M. Spinks, and G. Alici, "A 3D-printed omni-purpose soft gripper," *IEEE Trans. Robot.*, 2019, doi: 10.1109/TRO.2019.2924386.
[55] C. Tawk, G. M. Spinks, M. in het Panhuis, and G. Alici, "3D Printable vacuum-powered soft linear actuators," in *Proc. IEEE/ASME Int. Conf. Adv. Intell. Mech.*, 2019, pp. 50–55.
[56] R. Mutlu, C. Tawk, G. Alici, and E. Sariyildiz, "A 3D printed monolithic soft gripper with adjustable stiffness," in *Proc. 43rd Annu. Conf. IEEE Ind. Electron. Soc.*, 2017, pp. 6235–6240.

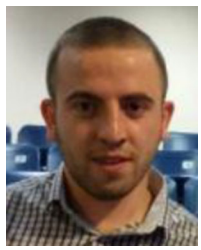

Charbel Tawk received the B.E. degree in mechanical engineering with high distinction from the Lebanese American University, Beirut, Lebanon, in 2016.

His research work at the University of Wollongong focuses on novel three-dimensional printable soft actuators and sensors.

Geoffrey M. Spinks received the Ph.D. degree from the University of Melbourne, Parkville, VIC, Australia, in 1990 for his work on the fracture behavior of unsaturated polyesters.

In December 1989, he was a Lecturer with the University of Wollongong (UOW), Wollongong NSW, Australia, where he is currently a Senior Professor. He has maintained a research interest in the mechanical behavior of polymers, especially actuator materials ("artificial muscles"). He has published more than 200 journal papers, including five papers in *Science*. As at December 2017, he had a total of 10300 citations and an "h-index" of 47. He has been actively involved in teaching and administration at UOW. He co-founded the Bachelor of Nanotechnology degree courses and has served as Discipline Advisor, research center Director and Associate Dean Research. He is currently the Challenge Leader of Manufacturing Innovation in UOW's Global Challenge program.

Marc in het Panhuis is from Grevenbicht, Limburg, The Netherlands. He received the Ph.D. degree from the Trinity College Dublin, University of Dublin, Dublin, Ireland.

He is a Chemical Engineer with the University of Twente, Enschede, The Netherlands, and a Physicist (with the University of Dublin). He is currently a Professor of materials science with the School of Chemistry and a Chief Investigator for electromaterials science with the Australian Research Council Centre of Excellence, University of Wollongong, Wollongong, NSW, Australia. His research interests include tough hydrogels, additive manufacturing (3D/4D Printing), edible/living electronics, soft robotics and 3D printed fins/surfboards for surfing.

Dr. Panhuis is an Associate Editor with the *Journal of Materials Chemistry B*.

Gursel Alici received the Ph.D. degree in robotics from the Department of Engineering Science, Oxford University, Oxford, U.K., in 1994.

He is currently a Senior Professor with the University of Wollongong, Wollongong, NSW, Australia, where he has been the Head of the School of Mechanical, Materials, Mechatronic, and Biomedical Engineering since 2011. His research interests include soft robotics, system dynamics and control, robotic drug delivery systems, novel actuation concepts for biomechatronic applications, robotic mechanisms and manipulation systems, soft and smart actuators and sensors, and medical robotics.

Dr. Alici was a Technical Editor for the IEEE/ASME TRANSACTIONS ON MECHATRONICS during 2008–2012. He has served on the international program committee of numerous IEEE/ASME International Conferences on Robotics and Mechatronics. He was the General Chair of the 2013 IEEE/ASME International Conference on Advanced Intelligent Mechatronics held in Wollongong, Australia. He was a member of the Mechatronics National Panel formed by the Institution of Engineers, Australia, from 2007 to 2017. He is the leader of Soft Robotics for Prosthetic Devices theme of the ARC Center of Excellence for Electromaterials Science. He was the recipient of the Outstanding Contributions to Teaching and Learning Award in 2010, the Vice-Chancellor's Interdisciplinary Research Excellence Award in 2013, and Vice-Chancellor's Award for Research Supervision in 2018 from the University of Wollongong. He has held a visiting professorship position at the Swiss Federal Institute of Technology, Lausanne (EPFL), in 2007 and 2010; City University of Hong Kong in 2014; University of Science and Technology of China in 2015; and University of British Columbia, Canada, in 2019.